Journal of Alloys and Compounds 779 (2019) 978–984

Contents lists available at ScienceDirect

Journal of Alloys and Compounds

journal homepage: http://www.elsevier.com/locate/jalcom

$Li_4Ti_5O_{12}$ epitaxial coating on $LiNi_{0.5}Mn_{1.5}O_4$ surface for improving the electrochemical performance through solvothermal-assisted processing

Jingzhong Zhao [a, *], Yurong Liu [a], Yi He [a], Kathy Lu [b]

[a] School of Materials and Engineering, Xi'an University of Technology, Xi'an, 710048, China
[b] Department of Materials Science and Engineering, Virginia Technology, Blacksburg, VA, 24061, USA

ARTICLE INFO

Article history:
Received 4 July 2018
Received in revised form
10 November 2018
Accepted 12 November 2018
Available online 15 November 2018

Keywords:
Lithium-ion batteries
$LiNi_{0.5}Mn_{1.5}O_4$
Epitaxial growth
Solvothermal method

ABSTRACT

During the charge-discharge of the $LiNi_{0.5}Mn_{1.5}O_4$ (LNMO) cathode in Li-ion batteries, Ni^{2+} and Mn^{2+} dissolve in the electrolyte to cause oxidative decomposition, which is the major cause for fast capacity fading and poor cycle performance. Reducing the direct contact area between the cathode material and the electrolyte is a direct solution to improve the cell performance. This paper focuses on a solvothermal method to coat the surface of $LiNi_{0.5}Mn_{1.5}O_4$ hollow microspheres with TiO_2 followed by TiO_2 conversion into $Li_4Ti_5O_{12}$ (LTO) using $LiOH{\cdot}H_2O$. The $Li_4Ti_5O_{12}$ coating layer synthesized by this method demonstrates epitaxial growth on the outer surface of $LiNi_{0.5}Mn_{1.5}O_4$. The LTO-coated LNMO cathode exhibits capacity retention of 88.1% after 100 cycles at 0.5C rate, much higher than 62.2% for the bare LNMO counterpart, at elevated temperature of 55 °C. In addition, the Li^+-ion mobility for the LTO-coated LNMO electrode is increased.

1. Introduction

In recent years, lithium-ion batteries are widely used in vehicles and portable electronics because of their high power and energy densities [1–9]. Spinel $LiNi_{0.5}Mn_{1.5}O_4$ (LNMO) cathode is widely preferred due to its excellent structural stability, high discharge capacity (theoretical specific capacity: 147 mAh/g), high operating voltage (4.7 V), abundance in nature, and low cost. However, the high operating voltage of LNMO accelerates the decomposition of the $LiPF_6$ electrolyte and the decomposition reaction of $LiPF_6$ in the electrolyte will produce HF. Subsequently, Ni^{2+} and Mn^{2+} dissolve into the electrolyte under the attack of the HF acid. Moreover, the highly delithiated Ni^{4+} ions with a high concentration and strong oxidization are present in the spinel LNMO cathode during charging and continue to oxidize the electrolyte on the cathode surface to form a solid-electrolyte interface (SEI) layer, which leads to fast capacity fading and poor cycle performance [10–18].

In order to solve the above problems, a direct solution is to treat the LNMO cathode material with a surface coating, thus reducing the direct contact area between the cathode material and the $LiPF_6$ electrolyte. Previously, LNMO has been modified by surface coating with $Li_4Ti_5O_{12}$(LTO) [19], Li_3PO_4 [20], Al_2O_3 [21], ZnO [22], SiO_2 [23], SnO_2 [24], and TiO_2 [25]. Among these materials, spinel $Li_4Ti_5O_{12}$ (LTO) is an important anode material for lithium ion batteries and experiences no structure changes during the insertion/extraction process of lithium ions. Thus, it is a zero-strain material with desirable structural stability. Moreover, both LTO and LNMO share the same spinel structure within the Fd-3m space group, which offers good lattice match between LTO and LNMO. Finally, the chemical diffusion coefficient of $Li_4Ti_5O_{12}$ (10^{-6} cm^2 s^{-1}) [14] is larger than that of $LiNi_{0.5}Mn_{1.5}O_4$ (10^{-9} -10^{-11} cm^2 s^{-1}) [15], which makes the diffusion of Li^+ ions across the cathode faster and can potentially increase the rate capability [26–28].

Currently, the studies on the LTO coating layer were almost always based on the traditional sol-gel technique. Because the coating layer is thick and non-uniform, it can easily peel off from the LNMO surface due to the fast and difficult-to-control hydrolysis rate of tetrabutyl titanate [29,30].

In this paper, we used a solvothermal method to coat the surface of spinel LNMO with LTO particles. The morphology, structure, and composition of the LTO-coated LNMO samples were investigated by X-ray diffraction (XRD), scanning electron microscopy (SEM),

* Corresponding author.
E-mail addresses: jzzhao@xaut.edu.cn (J. Zhao), 1294151844@qq.com (Y. Liu), 1024586470@qq.com (Y. He), klu@vt.edu (K. Lu).

https://doi.org/10.1016/j.jallcom.2018.11.152
0925-8388/

energy-dispersive X-ray spectroscopy (EDS), and transmission electron microscopy (TEM). The electrochemical performance of the surface-modified LNMO microspheres was evaluated by charge-discharge testing, cyclic voltammetry (CV), and electrochemical impedance spectroscopy (EIS).

2. Experimental

LNMO hollow microspheres fabrication: First, 15 mmol of $MnSO_4 \cdot H_2O$ and 5 mmol of $Ni(NO_3)_2 \cdot 6H_2O$ were dissolved in 560 mL mixed solution containing anhydrous ethanol and distilled water (in a volume ratio of 1: 1) at room temperature, which was denoted as solution A after thorough stirring. Second, 200 mmol of NH_4HCO_3 was dissolved in 280 mL of distilled water to form solution B after complete stirring. Subsequently, solution B was slowly poured into solution A and stirred for 2 h. After that, precipitation proceeded for 1 h at room temperature. After the reaction, the spherical precursor $(Ni_{0.25}Mn_{0.75})CO_3$ was collected by filtration, washing, and drying. Finally, the spherical precursor was decomposed at 400 °C for 5 h to obtain porous microspheres. Stoichiometric amounts of the as-prepared porous microspheres and $LiOH \cdot H_2O$ were mixed in ethanol before being dried and calcined at 800 °C for 15 h in air to produce hollow LNMO microspheres.

LNMO@TiO_2 microsphere fabrication: First, 0.1853 g of $Ti(OC_4H_9)_4$ was dispersed into 15 mL of ethanol, denoted as solution C after stirring; 1 mL of deionized water was added into 20 mL of ethanol, denoted as solution D after stirring. Then, solution D was slowly poured into solution C and stirred for 30 min to obtain a transparent solution. Subsequently, 0.95 g LNMO was dispersed into the transparent solution with ultrasonic treatment, sealed in a Teflon reactor and maintained at 150 °C for 8 h, and stirred every 30 min during the reaction process followed by centrifugation, washing, and drying. Finally, the sample was calcined at 700 °C for 2 h in air to obtain LNMO@TiO_2.

LTO@LNMO microsphere fabrication: The as-prepared LNMO@TiO_2 powder and 0.0192 g of $LiOH \cdot H_2O$ were added into ethanol, and the mixture was stirred until ethanol completely evaporated out. The dry mixture was then calcined at 700 °C for 2 h to obtain the final LTO@LNMO powder.

Powder X-ray diffraction (XRD) (7000, Shimadzu, Kyoto, Japan) was used to analyze the phase compositions of the cathode materials. Scanning electron microscopy (SEM) (JM6700F, JEOL, Tokyo, Japan) was used for morphology observation and transmission electron microscopy (TEM) (H-7650, Hitachi, Tokyo, Japan) was utilized to examine the thicknesses of the hollow microspheres and the coating layer.

The as-prepared active material (LNMO or LTO@LNMO), conductive carbon (acetylene black), and a polyvinylidene fluoride (PVDF) binder were mixed in a weight ratio of 80: 10: 10 in an N-methyl-2-pyrrolidone (NMP) solvent to form a slurry. The slurries were cast on an aluminum foil and dried in a vacuum at 120 °Cfor 12 h to form the cathodes. The cathodes were compacted with 10 MPa pressure and punched into 12 mm disks. The mass loading of the electrode material was 0.0020–0.0025 g. A lithium plate and a Celgard 2400 film were used as anode and separator, separately. The electrolyte was a solution of 1 M $LiPF_6$ dissolved in ethylcarbonate/dimethylcarbonate/diethylcarbonate (EC/DMC/DEC) (1:1:1 in volume). The assembly of CR2025 type cells was carried out in an Ar-filled glove box before electrochemical property testing.

The cells were galvanostatically charged-discharged at various current densities (1C = 147 mA/g) using the Land battery tester (CT2001A, Wuhan) in a voltage range of 3.5–4.9 V. The cyclic voltammetry (CV) test was performed using electrochemical workstation (CS350 in COM3) at a scan rate of 0.5 mV/s, and electrochemical impedance spectroscopy (EIS) was conducted with a working frequency from 0.1 Hz to 10^5 Hz and 10 mV perturbation amplitude.

3. Results

3.1. Crystal structure and morphology

Fig. 1 shows the XRD patterns of the LNMO and 5 wt% coated LTO@LNMO samples. The sharp XRD patterns mean that the LMNO powder has well-defined spinel structures with the space group of Fd-3m (JCPDS card no. 80–2162). The peaks at 35.6°, 43.2° and 62.8° correspond to the (311), (400), (440) planes of LTO. This indicates that the LTO has the spinel structure after the coating process. Meanwhile, the LTO-coated LNMO sample has sharper peaks, indicating that it has better crystallinity after the heat treatment with the continuous growth of the LNMO crystals.

The morphologies of the LNMO and LTO@LNMO powders are shown in Fig. 2. The LNMO particles in Fig. 2(a) have uniform shape and size, in the form of ~1.5 μm spheres. There is no obvious change in shape or size for the LNMO particles after coating LTO as shown in Fig. 2(b). As expected, fine LTO grains grow on the surface of the LNMO particles uniformly. The reason is that the stirring of the solvothermal process facilitates the suspension of the LNMO particles in the ethanol solution. $Ti(OC_4H_9)_4$ slowly decomposes into TiO_2 particles under high temperature and high pressure, which uniformly grow on the surface of the LNMO particles. When the TiO_2 coating layer reacts with $LiOH \cdot H_2O$, TiO_2 particles are converted into LTO. Fig. 2(c) shows that the LNMO particles are aggregated from ~100 nm primary particles, fine grains are uniformly distributed on the LNMO particles.

Fig. 3 shows the EDS pattern and the corresponding composition distribution maps of the elements in the LTO-coated LNMO sample. The atomic percent of Ti element is 1.43% and lower than the theoretical value (2.61%) as showed in Table 1. This may be because some of the LTO is not coated on the surface of the spherical particles. The EDS results also reveal uniform distribution of Ti on the particle surface, Mn and Ni elements homogeneously distribute in the selected region.

The TEM images of the LTO@LNMO samples are shown in Fig. 4. The average particle size is about 1.5 μm as shown in Fig. 4(a), consistent with the result in Fig. 3. The LNMO particles exhibit hollow spheres in this image. Fig. 4(b) is the enlarged image of Fig. 4(a), and the contrast difference between the LNMO particle

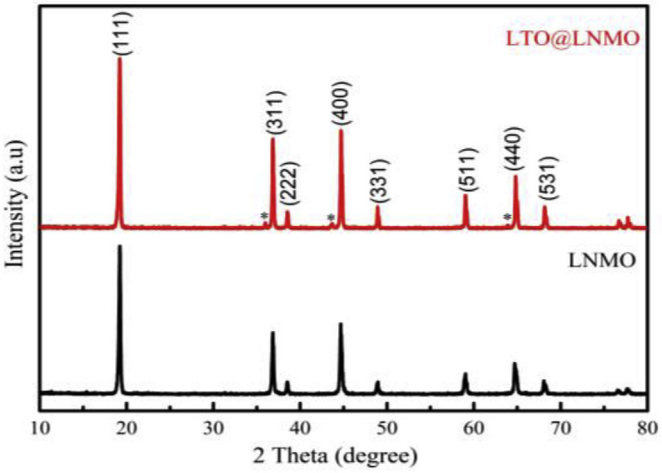

Fig. 1. XRD patterns of LNMO and LTO@LNMO.

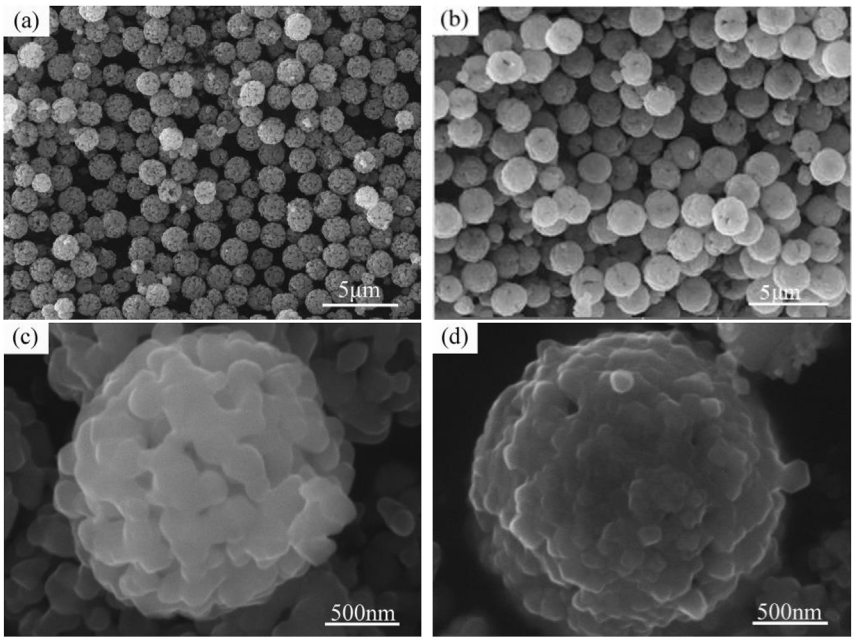

Fig. 2. SEM images of LNMO (a) at low magnification, (b) LTO@LNMO at low magnification, (c) LNMO at high magnification, and (d) LTO@LNMO at high magnification.

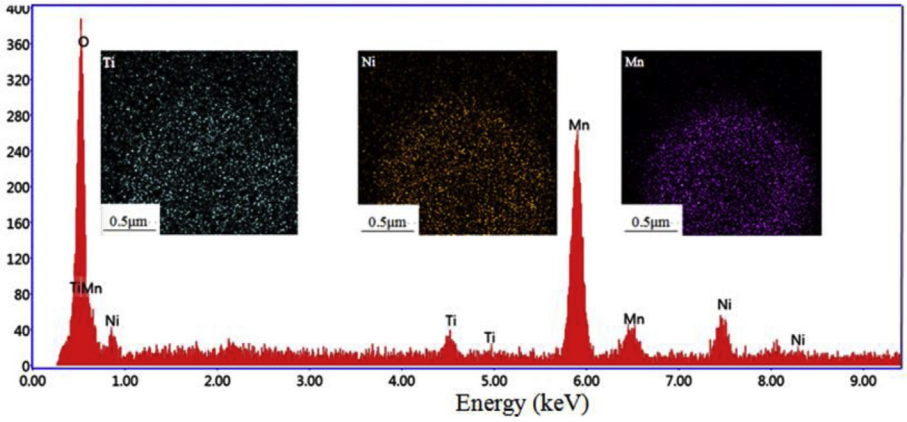

Fig. 3. EDS pattern and electron probe micro-analysis images for the Ti, Mn, Ni elements of the LTO@LNMO sample.

Table 1
EDS data of the LTO@LNMO material.

Element	Weight/%	Atomic/%
Ti k	2.59	1.43
Mn k	33.97	15.12
Ni K	12.14	5.05

and the coating layer can be seen with the dotted line exhibiting the interface layer of the LTO@LNMO particle. The thickness of the coating layer is estimated to be about 10 nm. To understand the crystal structure of the coating material, Fig. 4(c) shows the high resolution TEM image. There is a clear contrast difference between LNMO and LTO, marked with a dotted line, and the thickness of the coating layer is about 30 nm. The difference in contrast is due to the interplanar distance difference since both materials have a face-centered cubic spinel structure. The d-spacings are 0.24 nm and 0.25 nm respectively for the LNMO interior and the surface LTO region, corresponding to the lattice fringes of the (311) planes of LNMO and LTO, respectively. It can be inferred that LTO coats the surface of LNMO in the form of epitaxial growth, and the LTO coating layer has no obvious influence on the morphology and structure of the LNMO cathode material [31].

3.2. Electrochemical performance

Room and elevated temperature cycling performance of the bare and LTO-coated LNMO materials at current density of 0.5C and in the voltage range of 3.5–4.9 V are shown in Fig. 5(a) and (b). As shown in Fig. 5(a), the bare sample shows faster capacity fading, from 126.2 $mAh \cdot g^{-1}$ to 97.7 $mAh \cdot g^{-1}$ after 100 cycles with the capacity retention of only 77.4%. For the LTO-coated sample, the discharge capacity remains at 112.8 mAh g^{-1}, and the capacity retention is as high as 93.6% after 100 cycles. The cycling behaviors of the uncoated and coated-LNMO electrodes under 0.5C at 55 °C are illustrated in Fig. 5(b). Clearly, elevated temperature degrades the cycling stability. The capacity retention rates of the bare sample and the LTO-coated sample after 100 cycles both decrease, to 62.2%

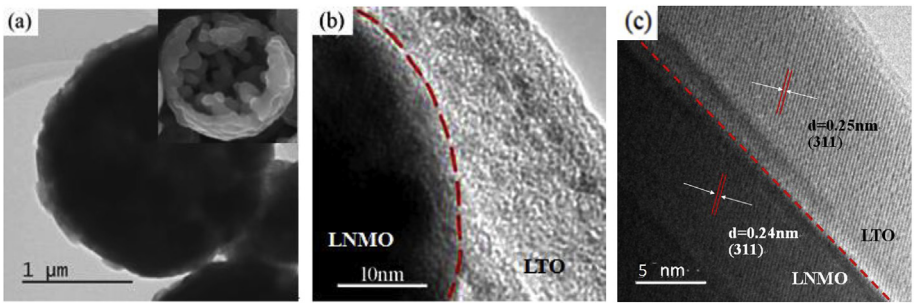

Fig. 4. TEM images of LTO@LNMO (a) at low magnification, (b) at high magnification, and (c) HR-TEM.

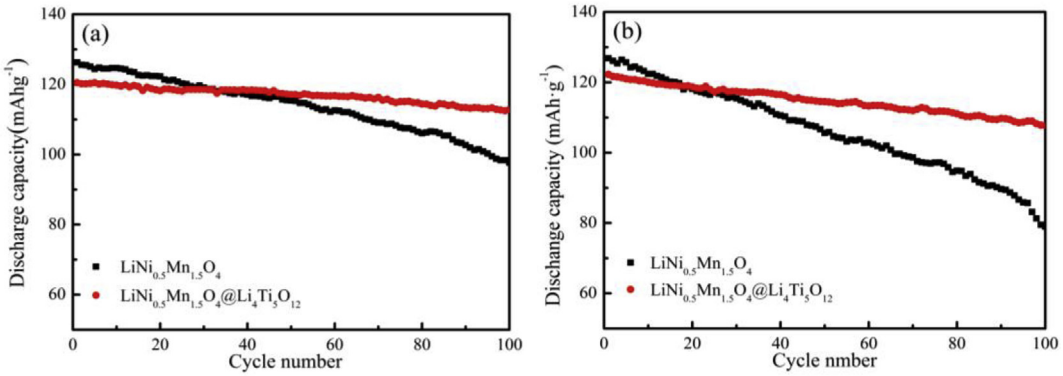

Fig. 5. Cycling performances of LNMO and LTO@LNMO cathodes cycled a 0.5C at (a) 25 °C, (b) 55 °C.

and 88.1%, respectively. Better capacity retention is observed for the LTO-coated LNMO sample, irrespective of the cycling temperature, which means that the LTO-coated layer can effectively prevent the direct contact between the electrolyte and the electrode material, reduce the side reactions on the surface of the sample and the dissolution of the cathode material.

The rate capabilities of the bare and LTO-coated LNMO electrodes at room and elevated temperatures with various C-rates are presented in Fig. 6. With the increase of the current density, the discharge capacities of the bare and LTO-coated LNMO electrodes both decrease. The rapid decrease in capacity is likely due to the high doses of Mn^{3+} ions in the bare LNMO. The LTO-coated LNMO electrode has a lower capacity than the uncoated cathode at low rates but a relatively higher capacity at high rates. From Fig. 6(a) we can see that the samples LNMO and LTO@LNMO exhibit discharge capacities of 134.8, 124, 115.3, 108.9, 91.2, 51.5 mAh·g^{-1} and 130.1, 122.6, 114.2, 111.8, 105.4, 91.4 mAh·g^{-1} at 0.2C, 0.5C, 1C, 2C, 5C and 10C, respectively. Compared with the bare LNMO electrode, the capacity at 10C for the LTO@LNMO electrode is from 38.2% to 70.3% of the capacity at 0.2C. The capacity recoveries for the bare LNMO and LTO-coated LNMO electrode are 89.4% and 98% respectively when the current rate is reversed from 10C back to 0.2C, showing possible structural degradation in the bare LNMO material during the high rate cycling because of the dissolution of the electrode material. As shown in Fig. 6(b), the discharge capacities of the LNMO and LTO@LNMO electrodes are both worse at 55 °C, especially at high rates. This is because the high temperature can speed up the dissolution of the electrode materials. And the capacity at 10C for the LNMO and LTO@LNMO electrodes are 23.4% and 66% of the capacity at 0.2C, respectively. The results illustrate that the LTO-coated LNMO electrode has a significant advantage on the rate capability and high temperature cycleability. Desirably, the

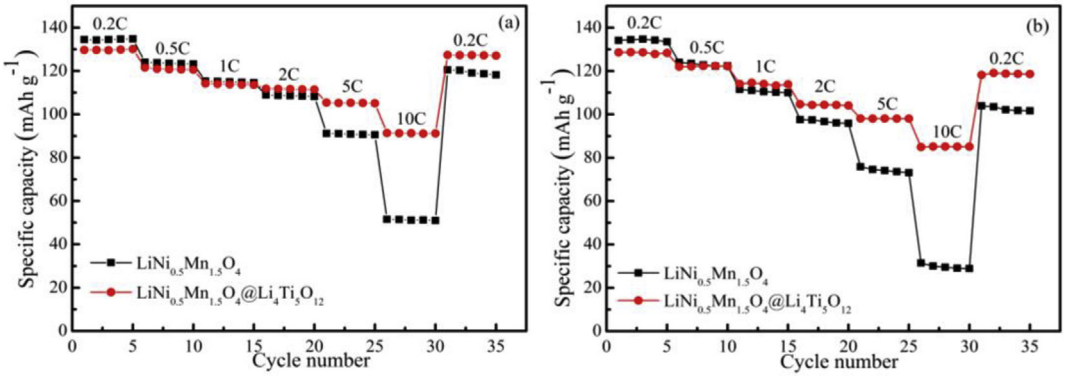

Fig. 6. Rate capabilities of LNMO and LTO@LNMO at (a) 25 °C, (b) 55 °C.

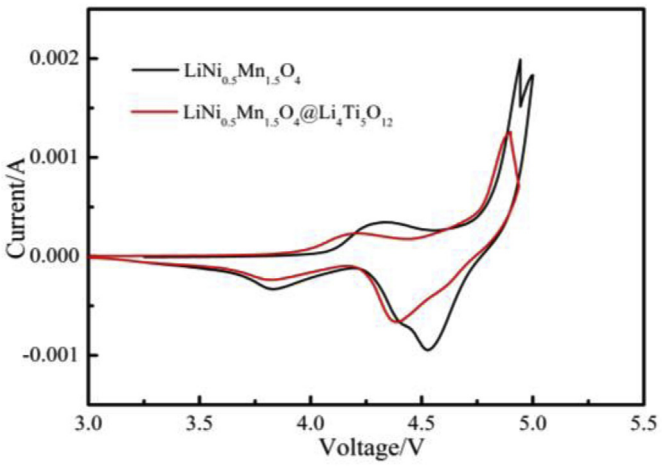

Fig. 7. Cyclic voltammetry of LNMO and LTO@LNMO.

Table 2
Values of the CV peaks for LNMO and LTO@LNMO.

samples		Φ_a/V	Φ_c/V	$\Phi_a-\Phi_c$/V
LNMO	Ni^{2+}/Ni^{3+}	4.939	4.399	0.54
	Ni^{3+}/Ni^{4+}	4.996	4.499	0.497
	Mn^{3+}/Mn^{4+}	4.298	3.822	0.476
LTO@LNMO	Ni^{2+}/Ni^{4+}	4.890	4.397	0.493
	Mn^{3+}/Mn^{4+}	4.188	3.838	0.35

structural degradation can be effectively suppressed with the LTO coating layer by suppressing the decomposition of the electrolyte and the Mn^{2+} in the LNMO spinel as well as offering higher Li^+-ion diffusion.

Fig. 7 shows the cyclic voltammetry (CV) results of the bare and LTO-coated LNMO after the 1st cycle at a scan rate of 0.5 mV/s between 3.5 and 5.0 V. The appearance of the peak near 4.1 V is attributed to the redox couple of Mn^{3+}/Mn^{4+}. It can be concluded that the bare and LTO-coated LNMO have a disordered spinel structure and belong to the Fd-3m space group. In Fig. 7, the peaks located near 4.8 V are due to the redox couples of Ni^{2+}/Ni^{3+} and Ni^{3+}/Ni^{4+} for the bare LNMO electrode and the redox couple Ni^{2+}/Ni^{4+} for the LTO-coated LNMO electrode. The oxidation peak splits into two separate peaks in the Fd3m spinel because the voltage difference between Ni^{2+}/Ni^{3+} and Ni^{3+}/Ni^{4+} redox couples is enhanced in the nonstoichiometric spinel [32,33]. The polarization degree can be measured by the potential difference ($\Delta\Phi$) between

Table 3
Charge transfer resistance (R_{ct}), σ values and Li^+ ion diffusion coefficients (D_{Li}) for LNMO and LTO@LNMO.

samples	R_{ct}/Ω	$\sigma/(\Omega/s^{1/2})$	D_{Li} (cm^2/s)
LNMO	204.6	246.76	1.15×10^{-14}
LNMO@LTO	150.8	125.25	8.14×10^{-14}

the anodic (Φ_a) and cathodic (Φ_c), which is listed in Table 2. The potential difference ($\Phi_a-\Phi_c$) of the LTO-coated LNMO electrode is lower than that of the bare LNMO. This observation suggests that the LTO-coated layer is beneficial to the reversible insertion/extraction kinetics of lithium ions and can enhance the reversibility. Moreover, this improvement can be ascribed to the coated LTO on the electrode surface, which suppresses the Mn^{3+} ions from dissolving into the electrolyte in the 4.1 V region.

To further investigate the effects of the LTO-coated LNMO on the electrochemical performance, electrochemical impedance spectroscopy (EIS) was carried out under a fully discharged state after 1 cycle. Fig. 8 (a) shows that all the Nyquist plots have the same shape, consisting of a semicircle and a linear slop. The slope at low-frequency is due to the Warburg diffusion, which is the resistance of Li^+ diffused into the active material. The semicircle at high-frequency indicates the charge transfer resistance (R_{ct}) during the electrochemical reaction. Based on the fitting results of the Nyquist plots through the ZView software, the R_{ct} of LNMO and the LTO-coated LNMO are 204.6Ω and 150.8Ω, respectively, as shown in Table 2, indicating that the LTO coating can decrease the charge transfer resistance. This is believed to result from the LTO coating, which can suppress the reaction between the cathode surface and the electrolyte during cycling.

The Li^+ ion diffusion coefficient (D_{Li}) can be calculated from the following equations [34–36]:

$$D_{Li} = 0.5\left(\frac{RT}{An^2F^2\sigma C}\right)^2 \quad (1)$$

$$Z' = R_e + R_{ct} + \sigma\omega^{-1/2} \quad (2)$$

$$C = n/V = (m/M)/V = (\rho V/M)/V = \rho/M \quad (3)$$

where R is the gas constant (8.314 J/(mol·K)), T is the temperature (298 K), A is the surface area of the electrode ($A = 2\pi r^2 = 1.13\ cm^2$), n is the number of electrons per molecule during oxidation (n = 1), F is the Faraday's constant (96500C/mol), C is the molar concentration of Li^+ ions and can be calculated from the density and the molecular weight of the materials ($C_{LNMO} = 0.0063\ mol\ cm^{-3}$,

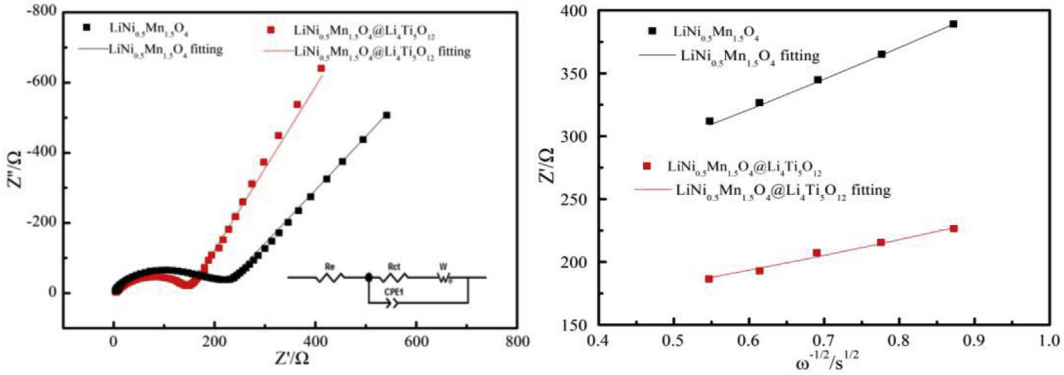

Fig. 8. EIS spectra and fitting-figures (a) and Z'-$\omega^{-1/2}$ graphs in low-frequency region (b) of LNMO and LTO@LNMO.

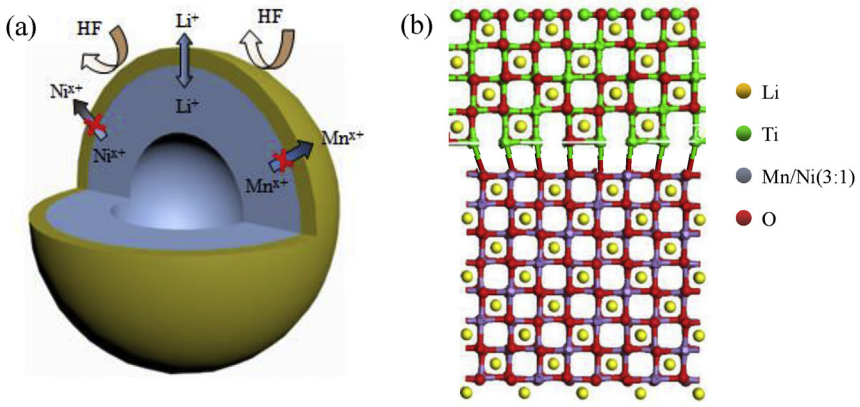

Fig. 9. Model of LTO@LNMO (a) Coating structure (b) epitaxial growth structure.

$C_{LTO@LNMO} = 0.0046\ mol\ cm^{-3}$), and σ is the Warburg factor. The Z'-$\omega^{-1/2}$ plots of the LNMO and LTO-coated LNMO cathodes are presented in Fig. 8 (b), from which the values for σ are obtained. Thus, we can obtain the values for Li^+ ion diffusion coefficient (D_{Li}), as listed in Table 3. It can be seen that the Li^+ ion diffusion coefficient for the LTO-coated LNMO electrode ($8.14 \times 10^{-14}\ cm^2/s$) is higher than that of the LNMO electrode ($1.15 \times 10^{-14}\ cm^2/s$), indicating that the LTO-coated LNMO electrode has higher Li^+ ion diffusion mobility than the bare LNMO electrode, which could partly explain the higher rate capability of the LTO-coated samples.

Based on the EIS analysis, it can be concluded that the LTO-coated LNMO cathode material exhibits lower charge transfer resistance and larger Li^+ diffusion coefficient, implying its better electrochemical performance.

4. Discussion

The model for the LTO@LNMO particles can be shown in Fig. 9(a). During the charge-discharge process, the decomposition reactions of $LiPF_6$ in the electrolyte are:

$$LiPF_6 \rightarrow LiF + PF_5 \quad (4)$$

$$PF_5 + H_2O \rightarrow POF_3 + 2HF \quad (5)$$

$$POF_3 + 3H_2O \rightarrow H_3PO_4 + 3HF \quad (6)$$

The decomposition of the electrolyte produces HF, and the LTO coating layer can prevent the direct contact between the cathode material and HF and reduce the scavenging of HF on the host material, suppressing the dissolution of Mn and Ni. As a result, the capacity fading caused by the dissolution of the cathode during the charge–discharge process can be effectively slowed down [37]. Meanwhile, the rate capability of the LTO@LMNO sample is increased because of the much higher Li^+-ion mobility in LTO. The epitaxial growth of LTO along the (100) plane of the cathode material is shown in Fig. 9(b). The specific process can be understood as follows. TiO_2 powders are dispersed homogeneously on the surface of the LNMO particles during the solvothermal pre-coating treatment. Some Li^+ ions on the surface of the LNMO particles diffuse into the interface layer, and TiO_2 is converted into the LTO interface layer by reacting with Li^+. Moreover, LTO shares the same spinel structure with LNMO. The lattice parameters for LTO and LNMO are 8.3588 and 8.1730 Å, respectively and the lattice mismatch between LTO and LNMO is small. The Ti in LTO combines with the O in the host material LNMO to form the Ti–O bond, Ni and Mn in the host material LNMO combines with the O in LTO to form the Mn–O bond and Ni–O bond. Thus, an epitaxial transition layer is formed. When mixed with LiOH, LTO is formed after annealing [27].

5. Conclusions

A homogeneous $Li_4Ti_5O_{12}$ epitaxial coating layer on $LiNi_{0.5}Mn_{1.5}O_4$ surface was successfully synthesized by a solvothermal method. The $Li_4Ti_5O_{12}$ coating was utilized to improve the electrochemical performance of spinel $LiNi_{0.5}Mn_{1.5}O_4$ cathode materials, including cycling stability and high temperature cycleability, without changing the crystal structure of the $LiNi_{0.5}Mn_{1.5}O_4$ electrode. By the CV and EIS analyses it shows that the $Li_4Ti_5O_{12}$ coating layer can suppress the reaction between the cathode surface and the electrolyte and benefit the reversible insertion/extraction kinetics of Li^+ ions, subsequently leading to smaller polarization degree, lower charge transfer resistance and higher lithium ion diffusion coefficient.

References

[1] M.S. Whittingham, Lithium battery and cathode materials, Chem. Rev. 104 (2004) 4271–4302.
[2] C. Hendricks, N. Williard, S. Mathew, A failure modes, mechanisms, and effects analysis (FMMEA) of lithium-ion batteries, J. Power Sources 297 (2015) 13–120.
[3] A. Eftekhari, Ordered mesoporous materials for lithium-ion batteries, Microporous Mesoporous Mater. 243 (2017) 355–369.
[4] M.J. Uddin, P.K. Alaboina, S.J. Cho, Nanostructured cathode materials synthesis for lithium-ion batteries, Mater. Today Energy 5 (2017) 138–157.
[5] B. Diouf, R. Pode, Potential of lithium-ion batteries in renewable energy, Renew. Energy 76 (2015) 375–380.
[6] J.L. Li, C.B. Cao, X.Y. Xu, $LiNi_{1/3}Co_{1/3}Mn_{1/3}O_2$ hollow nano-micro hierarchical microspheres with enhanced performances as cathodes for lithium-ion batteries, J. Mater. Chem. A. 1 (2013) 11848–11852.
[7] R.Y. Tian, H.Q. Liu, Y. Jiang, Drastically enhanced high-rate performance of carbon coated $LiFePO_4$ nanorods using a green chemical vapor deposition (CVD) method for Lithium ion battery: a selective carbon coating process, ACS Appl. Mater. Interfaces 7 (2015) 11377–11386.
[8] K.H. Prasad, S. Vinoth, A. Ratnakar, Structural and electrical conductivity studies of spinel $LiMn_2O_4$ cathode films grown by RF sputtering, Mater. Today 3 (2016) 4046–4051.
[9] H.D. Liu, J. Wang, X.F. Zhang, Morphological evolution of high-voltage spinel $LiNi_{0.5}Mn_{1.5}O_4$ cathode materials for lithium-Ion batteries: the critical effects of surface orientations and particle size, ACS Appl. Mater. Interfaces 8 (2016) 4661–4675.
[10] R. Aswathy, T. Kesavan, K.T. Kumaran, Octahedral high voltage LiNi0.5Mn1.5O4 spinel cathode: enhanced capacity retention of hybrid aqueous capacitors with nitrogen doped graphene, J. Mater. Chem. A. 3 (2015) 12386–12395.
[11] Y.J. Gu, Y. Li, Y.B. Chen, Comparison of Li/Ni antisite defects in Fd-3m and P4332 nanostructured LiNi0.5Mn1.5O4 electrode for Li-ion batteries, Electrochim. Acta 213 (2016) 368–374.

[12] J.H. Kim, N.P.W. Pieczonka, Z.C. Li, Understanding the capacity fading mechanism in $LiNi_{0.5}Mn_{1.5}O_4$/graphite Li-ion batteries, Electrochim. Acta 90 (2013) 556–562.
[13] J.H. Kim, A. Huq, M.F. Chi, Pieczonka, et al., Integrated nano-domains of disordered and ordered spinel phases in $LiNi_{0.5}Mn_{1.5}O_4$ for Li-Ion batteries, Chem. Mater. 26 (2014) 4377–4386.
[14] Z. Zhu, D. Zhang, H. Yan, Precise preparation of high performance spherical hierarchical $LiNi_{0.5}Mn_{1.5}O_4$ for 5 V lithium ion secondary batteries, J. Mater. Chem. A. 1 (2013) 5492–5496.
[15] C.Y. Zhu, T. Akiyama, Designed synthesis of $LiNi_{0.5}Mn_{1.5}O_4$ hollow microspheres with superior electrochemical properties as high-voltage cathode materials for lithium-ion batteries, RSC Adv. 4 (2014) 10151–10156.
[16] W.K. Shin, Y.S. Lee, D.W. Kim, Study on the cycling performance of LiNi0.5Mn1.5O4 electrodes modified by reactive SiO2 nanoparticles, J. Mater. Chem. A. 2 (2014) 6863–6869.
[17] J. Chong, J.P. Zhang, H.M. Xie, High performance LiNi0.5Mn1.5O4 cathode material with a bi-functional coating for lithium ion batteries, RSC Adv. 6 (2016) 19245–19251.
[18] M.Q. Xu, L. Zhou, Y.N. Dong, Development of novel lithium borate additives for designed surface modification of high voltage LiNi0.5Mn1.5O4 cathodes, Energy Environ. Sci. 9 (2016) 1308–1319.
[19] M. Sachs, M. Gellert, M. Chen, $LiNi_{0.5}Mn_{1.5}O_4$ high-voltage cathode coated with $Li_4Ti_5O_{12}$: a hard X-ray photoelectron spectroscopy (HAXPES) study, Phys. Chem. Chem. Phys. 17 (2015) 31790–31800.
[20] S. Yubuchi, Y. Ito, T. Matsuyama, 5 V class LiNi0.5Mn1.5O4 positive electrode coated with Li3PO4 thin film for all-solid-state batteries using sulfide solid electrolyte, Solid State Ionics 285 (2016) 79–82.
[21] J.W. Kim, D.H. Kim, D.Y. Oh, Surface chemistry of $LiNi_{0.5}Mn_{1.5}O_4$ particles coated by Al_2O_3 using atomic layer deposition for lithium-ion batteries, J. Power Sources 274 (2015) 1254–1262.
[22] Y.K. Sun, C.S. Yoon, I.H. Oh, Surface structural change of ZnO-coated $LiNi_{0.5}Mn_{1.5}O_4$ spinel as 5 V cathode materials at elevated temperatures, Electrochim. Acta 48 (2003) 503–506.
[23] Y.K. Fan, J.M. Wang, Z. Tang, Effects of nanostructured SiO_2 coating on the surface of $LiNi_{0.5}Mn_{1.5}O_4$ cathode materials for high-voltage Li-ion batteries, Electrochim. Acta 52 (2007) 3870–3875.
[24] F. Ma, F.S. Geng, A.B. Yuan, Facile synthesis and characterization of a SnO_2-modified $LiNi_{0.5}Mn_{1.5}O_4$ high-voltage cathode material with superior electrochemical performance for lithium ion batteries, Phys. Chem. Chem. Phys. 19 (2017) 9983–9991.
[25] S. Tao, F.J. Kong, C.Q. Wu, Nanoscale TiO2 membrane coating spinel LiNi0.5Mn1.5O4 cathode material for advanced lithium-ion batteries, J. Alloys Compd. 705 (2017) 413–419.
[26] Y.B. Shen, M. Søndergaard, M. Christensen, Iversen, Solid State formation mechanism of Li4Ti5O12 from an anatase TiO2 source, J. Mater. Chem. 26 (2014) 3679–3686.
[27] T.F. Yi, Z.K. Fang, Y. Xie, Rapid charge–discharge property of Li4Ti5O12–TiO2 nanosheet and nanotube composites as anode material for power lithium-ion batteries, ACS Appl. Mater. Interfaces 6 (2014) 20205–20213.
[28] T.F. Yi, S.F. Yang, Y. Xie, Recent advances of Li4Ti5O12 as a promising next generation anode material for high power lithium-ion batteries, J. Mater. Chem. A. 3 (2015) 5750–5777.
[29] T.F. Yi, J. Shu, Y.F. Zhu, Structure and electrochemical performance of $Li_4Ti_5O_{12}$-coated $LiMn_{1.4}Ni_{0.4}Cr_{0.2}O_4$ spinel as 5V materials, Electrochem. Commun. 11 (2009) 91–94.
[30] D.Q. Liu, X.Q. Liu, Z.Z. He, The elevated temperature performance of $LiMn_2O_4$ coated with $Li_4Ti_5O_{12}$ for lithium ion battery, Mater. Chem. Phys. 105 (2007) 362–366.
[31] J.L. Li, Y.Q. Zhu, L. Wang, Lithium titanate epitaxial coating on spinel lithium manganese oxide surface for improving the performance of lithium storage capability, ACS Appl. Mater. Interfaces 6 (2014) 18742–18750.
[32] L. Wang, D. Chen, J.F. Wang, G.J. Liu, W. Wu, G.H. Liang, Synthesis of $LiNi_{0.5}Mn_{1.5}O_4$ cathode material with improved electrochemical performances through a modified solid-state method, Powder Technol. 292 (2016) 203–209.
[33] W. Wu, X. Qin, J.L. Guo, J.F. Wang, H.Y. Yang, L. Wang, Influence of cerium doping on structure and electrochemical properties of $LiNi_{0.5}Mn_{1.5}O_4$ cathode materials, J. Rare Earths 35 (2017) 888–894.
[34] J. Deng, Y.L. Xu, L.L. Xiong, Improving the fast discharge performance of high-voltage $LiNi_{0.5}Mn_{1.5}O_4$ spinel by Cu^{2+}, Al^{3+}, Ti^{4+} tri-doping, J. Alloys Compd. 677 (2016) 18–26.
[35] J.F. Wang, D. Chen, W. Wu, L. Wang, G.C. Liang, Effects of Na^+ doping on crystalline structure and electrochemical performances of $LiNi_{0.5}Mn_{1.5}O_4$ cathode material, Trans. Nonferrous Metals Soc. China 27 (2017) 2239–2248.
[36] X.Y. Wang, H. Hao, J.L. Liu, T. Huang, A.S. Yu, A novel method for preparation of macroporous lithium nickel manganese oxygen as cathode material for lithium ion batteries, Electrochim. Acta 56 (2011) 4065–4069.
[37] S. Kim, M. Kim, I. Choi, Quercetin as electrolyte additive for $LiNi_{0.5}Mn_{1.5}O_4$ cathode for lithium-ion secondary battery at elevated temperature, J. Power Sources 336 (2016) 316–324.